Electronic Supplementary Information

Vacancy defective perovskite $Na_{0.85}Ni_{0.45}Co_{0.55}F_{3.56}$ nanocrystal anode for advanced lithium-ion storage driven by surface conversion and insertion hybrid mechanisms

Wei Shi [a], Rui Ding,*[a] Qilei Xu [a], Tong Yan [a], Yuxi Huang [a], Caini Tan [a], Xiujuan Sun [a], Ping Gao [a], and Enhui Liu [a]

[†]Key Laboratory of Environmentally Friendly Chemistry and Applications of Ministry of Education, College of Chemistry, Xiangtan University, Hunan 411105, P.R. China

[*] E-mails: drm8122@163.com; drm8122@xtu.edu.cn (R. Ding);

Tel: +86 731 58292202; Fax: +86 731 58292251

Table of Contents

Figure S13. CV plots for the first three cycles at 0.3 mV s^{-1}, GCD curves for the first five cycles at 0.1 A g^{-1}, GCD curves at 0.1-3.2 A g^{-1}, specific capacity and Coulombic efficiency at 0.1-3.2 A g^{-1} and cycling behavior at 2 A g^{-1} of five types of positive electrodes: AC (a-e), LFP (f-j), AC+LFP (k-o), KS6 (p-t) and KS6+LFP (u-y).

Figure S14. Performance of LICs (NNCF//AC, NNCF//AC+LFP), Li-DIBs (NNCF//KS6, NNCF//KS6+LFP) and LIB (NNCF//LFP) under low (-20 ℃) and high (40 ℃) temperature: CV plots at 10 mV s^{-1} (a, d, g, j), GCD curves at 1 A g^{-1} (b, e, h, k), Ragone plots (c, i) and cycling behavior (f, l).

Figure S15. CV window at 10 mV s^{-1}, CV plots at 10-160 mV s^{-1} and GCD curves at 0.5-16 A g^{-1} under room temperature (25 ^{o}C) of LICs, Li-DIBs and LIBs in this work: NNCF//AC (a-c), NNCF//LFP (d-f), NNCF//AC+LFP (g-i), NNCF//KS6 (j-l) and NNCF//KS6+LFP (m-o).

Figure S16. CV window at 10 mV s^{-1}, CV plots at 10-160 mV s^{-1} and GCD curves at 0.5-16 A g^{-1} under high temperature (40 ^{o}C) of LICs, Li-DIBs and LIBs in this work: NNCF//AC (a-c), NNCF//LFP (d-f), NNCF//AC+LFP (g-i), NNCF//KS6 (j-l) and NNCF//KS6+LFP (m-o).

Figure S17. CV window at 10 mV s^{-1}, CV plots at 10-160 mV s^{-1} and GCD curves at 0.5-16 A g^{-1} under low temperature (-20 ^{o}C) of LICs, Li-DIBs and LIBs in this work: NNCF//AC (a-c), NNCF//LFP (d-f), NNCF//AC+LFP (g-i), NNCF//KS6 (j-l) and NNCF//KS6+LFP (m-o).

Table S1. Chemicals, agents and materials used in the study.

Table S2. Specific capacity and cycling retention of the NNCF (Ni:Co=1:0~0:1) electrodes.

Table S3. Specific capacity cycling retention of AC, LFP, AC+LFP (1:1), KS6 and KS6+LFP (1:1) electrodes.

Table S4. Performance summary of the LICs, Li-DIBs and LIBs in the study under room temperature (25 ^{o}C).

Table S5. Performance summary of the LICs, Li-DIBs and LIBs in the study under high (40 ^{o}C) and low (-20 ^{o}C) temperatures.

Table S6. A comparison for the performance of the NNCF//AC and NNCF//AC+LFP LICs in the study with some reported LICs.

Table S7. A comparison for the performance of the NNCF//LFP LIB in the study with some reported LIBs.

Table S8. A comparison for the performance of the NNCF//KS6 and NNCF//KS6+LFP Li-DIBs in the study with some reported Li-DIBs.

References.

Experimental Procedures

Synthesis of NNCF materials

The chemicals in the experiment were of analytical level (A.R.) without further purification (Table S1). The NNCF samples were synthesized via a facile one-pot solvothermal route. Take the procedure of NNCF (1:1) for an example. Firstly, 1 mmol $NiCl_2•6H_2O$, 1 mmol $CoCl_2•6H_2O$, 5 mmol NaF and 0.20 g PVP-K30 were dissolved into 40 ml ethylene glycol (EG) solvents, and the mixture was magnetically stirred thoroughly and dispersed well in an ultrasonic bath for 30 min at 100 W power condition. Secondly, the mixture was transferred into a 50 ml Teflon-lined stainless steel autoclave, which was heated at 180 ^oC for 24 h in an electric oven, and then cooled down naturally. Next, the yielded precipitates were collected by centrifugal filtration along with absolute alcohol washing for several times. Finally the precipitates were dried overnight at 95 ^oC to obtain the products. The other four NNCF samples (1:0, 3:1,1:3 and 0:1) were also synthesized as the procedure described above except by using different stoichiometric molar ratios of Ni:Co at the beginning.

Characterizations

The phases and crystallinity properties were determined by X-ray diffraction (XRD). The morphology and size of particles were analyzed by scanning electron microscopy (SEM) and transmission electron microscopy (TEM). The crystalline microstructures were resolved by the high-resolution TEM (HRTEM) and selected area electron diffraction (SAED). The element composition and distribution were measured by the X-ray energy dispersive spectra (EDS), inductively coupled plasma-optical emission spectrometer (ICP-OES) and mapping. The surface chemical compositions and electronic structures were checked by X-ray photoelectron spectra (XPS). The specific surface area and pore volume/pore size distribution were examined by nitrogen isothermal sorptions with Brunauer-Emmett-Teller (BET) and Barrett-Joyner-Halenda (BJH) methods, respectively.

Electrochemical measurements

The electrodes were prepared by the following two steps: firstly, A well-dispersed mixture of 70 wt% active materials (as-synthesized NNCF (1:0-0:1) or commercial AC, YEC-8B or graphite (KS6) or $LiFePO_4$ (LFP) or AC+LFP (1:1 in weight) or KS6+LFP (1:1 in weight)), 20 wt% acetylene black (AB) conductive agent and 10 wt% polyvinylidene fluoride binder (PVDF, which was dissolved in into the

N-methyl-2-pyrrolidone (NMP)) were casted onto the current collectors (Cu foil and carbon-coated Al foil were used for the collectors of anode and cathode respectively), and followed by drying in a vacuum oven at 110 °C for 12 h; secondly, the electrodes were punched into disks with diameter of 12 mm, and the mass loading of active materials was about 1.2 mg cm^{-2}. The electrochemical performances were examined by cyclic voltammetry (CV) and galvanostatic charge-discharge (GCD) tests via CHI660E electrochemical working stations and Neware-CT-4008 testers. Tests for electrodes (NNCF, AC, LFP, AC+LFP, KS6, KS6+LFP) were conducted in half-cells by using the type 2032 coin cells with a certain working electrode (WE), a Li plate as both counter electrode (CE) and reference electrode (RE), and one piece of glass fiber (GF) as separator. Tests for LICs (NNCF//AC, NNCF//AC+LFP), Li-DIBs (NNCF//KS6, NNCF//KS6+LFP) and LIBs (NNCF//LFP) were conducted via full-cells with type 2032 coin cells with equal mass ratios of electrode active materials, and the NNCF anode was precharged at 0.1 A g^{-1} for 3.5 cycles before assembling the cells. The electrolytes used in the study were 1 M $LiPF_6$ dissolved in the mixed solvents of ethylene carbonate (EC), dimethyl carbonate (EMC) and dimethyl carbonate (DMC) (1:1:1 in volume) with 1% vinylene carbonate (VC) additives (LBC-305-01, CAPCHEM). All cell assemblies were performed in an high pure Ar-filled dry glovebox (MIKROUNA, O_2 and H_2O<0.1 ppm) and all tests were carried out at room temperature (about 25 °C) except the assigned tests under high (40 °C) and low (-20 °C) temperatures. (The above-mentioned chemicals, agents and materials are listed in the Table S1).

Calculations for C_m, E_m, P_m

The specific capacity (C_m, mAh g^{-1}), energy density (E_m, Wh kg^{-1}) for LICs, energy density (E_m, Wh kg^{-1}) for Li-DIBs and LIBs, and power density (P_m, kW kg^{-1}) were calculated according to the Equations S1-S4.

$$C_m = Q / m \quad (1)$$

$$E_m \text{ (Capacitor)} = 0.5\,(C_m \triangle V) \quad (2)$$

$$E_m \text{ (Battery)} = (C_m V) \quad (3)$$

$$P_m = 3.6\, E_m / t_d \quad (4)$$

Where m, Q, $\triangle V$, V and t_d refer to the mass of active materials (g) (for half cells, it means the mass of active materials of anode or cathode; for LICs, Li-DIBs and LIBs full cells, it means the total masses of active materials of anode and cathode), charge quantity (mAh) (for anode, it means the charge quantity of charging part; for cathode and full cells, it refers to the charge quantity of discharging part), potential window (V), plateau potential of the discharging plots (V) and discharging time (s) , respectively.

Results and Discussion

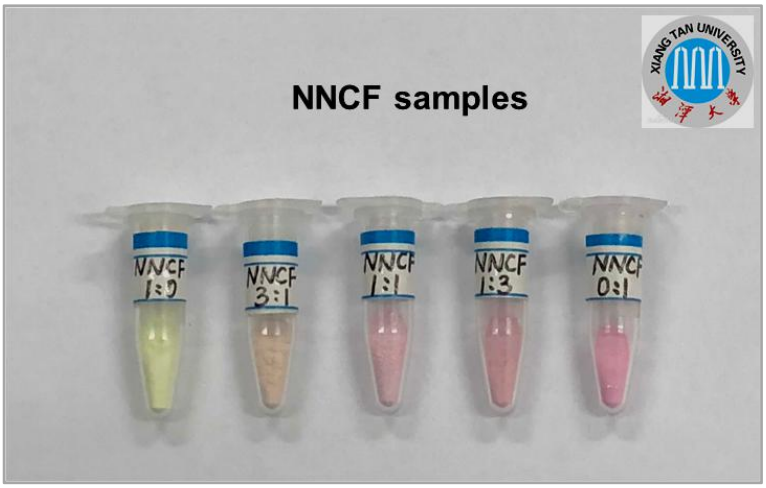

Figure S1. A picture of NNCF samples (Ni:Co=1:0~0:1).

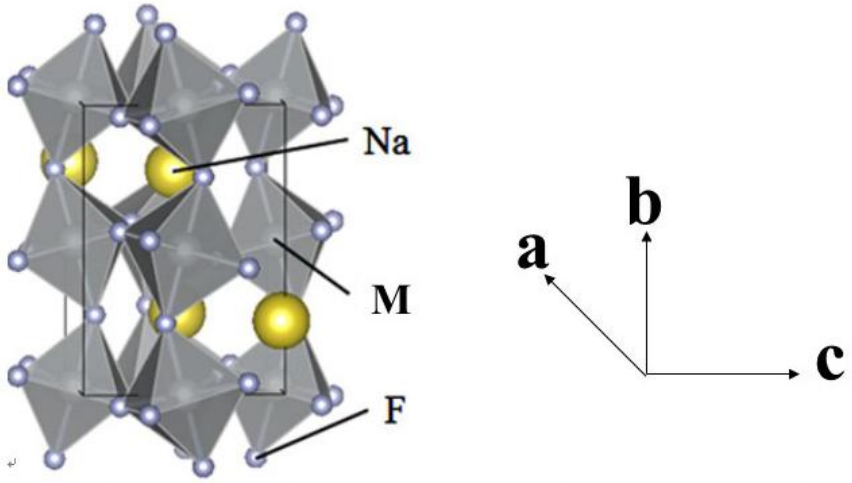

Sample	ICCD-PDF	Cyrstal system	Space group	Cell (axbxc)/Å^3
$NaNiF_3$	81-0953	Orthorhombic	Pbnm (62)	5.366x5.553x7.695
$NaCoF_3$	81-0955	Orthorhombic	Pbnm (62)	5.422x5.606x7.786

Figure S2. The crystal structures of perovskite $NaMF_3$ and detailed crystalline parameters for $NaNiF_3$ and $NaCoF_3$.

As shown in Fig. S2, the orthorhombic $NaMF_3$ is formed by alternatively stacking up Na ion layer and MX_3 cluster layer along the b-axis, and this MX_3 cluster layer is constructed by MX_6 octahedra which link to neighbor octahedra by edge-and corner-sharing along the a- and c-axes, respectively.

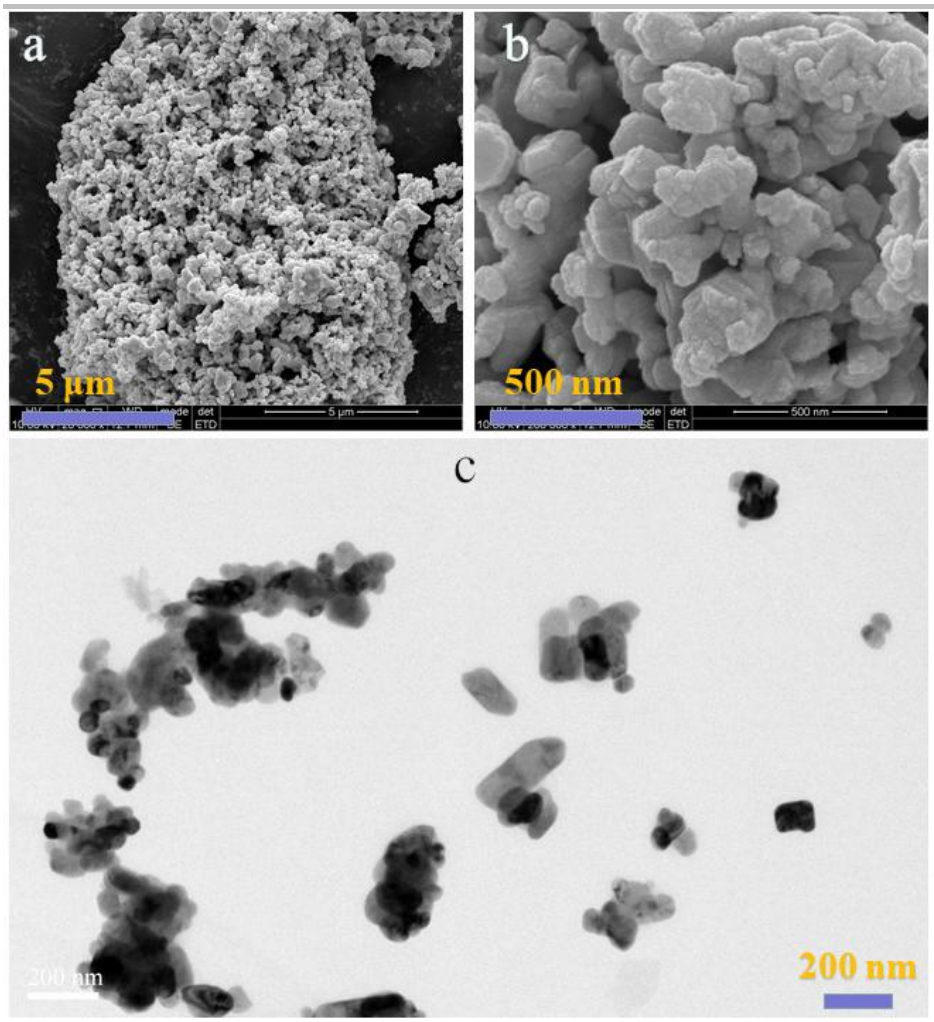

Figure S3. SEM and TEM images of NNCF (1:1) Sample.

The SEM images (Fig. S3a-S3b) and TEM image (Fig. S3c) of NNCF (1:1) sample exhibit a rectangular nanocrystal morphology with the size of 100-200 nm.

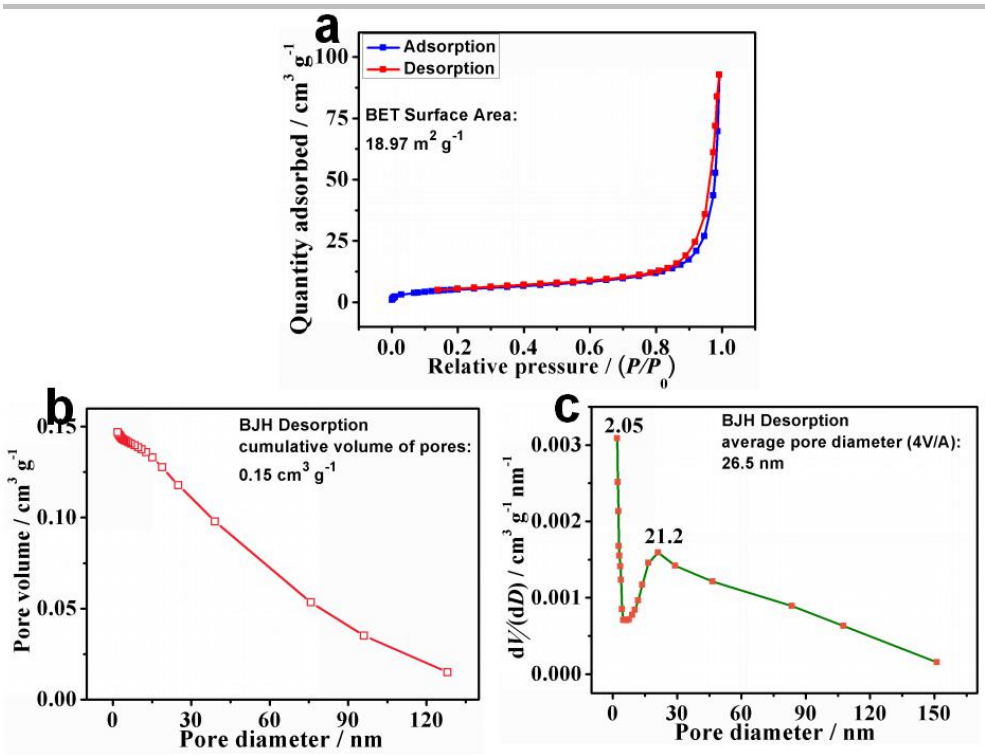

Figure S4. Nitrogen sorption isothermals (a), pore volume (b) and pore size distribution (c) of NNCF (1:1) Sample.

As depicted in Fig. S4, the specific surface area, cumulative pore volume and average pore diameter are 18.97 m^2 g^{-1}, 0.15 cm^3 g^{-1} and 26.5 nm respectively, with the dominant pore size located at 2.05 and 21.2 nm.

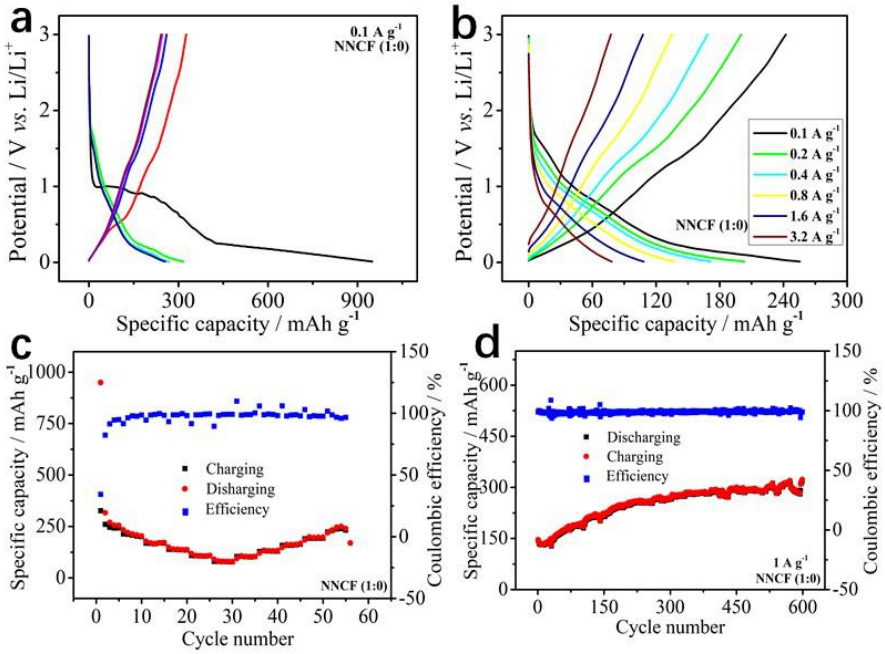

Figure S5. Performance of NNCF (1:0) electrode: GCD curves for the first five cycles at 0.1 A g^{-1} (a), GCD curves at 0.1-3.2 A g^{-1} (b), specific capacity and Coulombic efficiency at 0.1-3.2 A g^{-1} (c), and cycling behavior at 1 A g^{-1} (d).

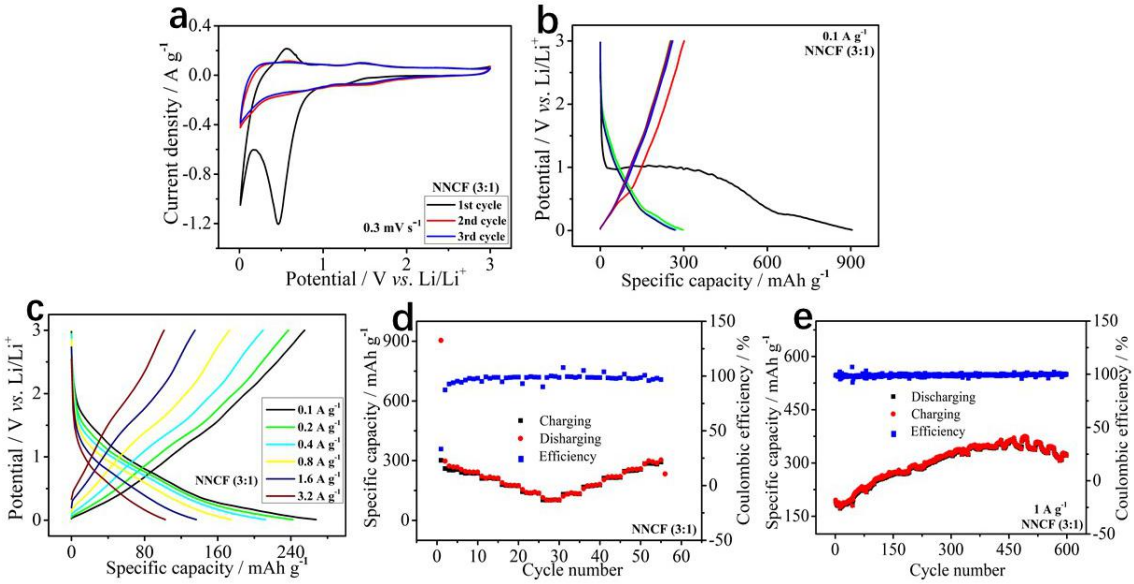

Figure S6. Performance of NNCF (3:1) electrode: CV plots for the first three cycles at 0.3 mV s^{-1} (a), GCD curves for the first five cycles at 0.1 A g^{-1} (b), GCD curves at 0.1-3.2 A g^{-1} (c), specific capacity and Coulombic efficiency at 0.1-3.2 A g^{-1} (d), and cycling behavior at 1 A g^{-1} (e).

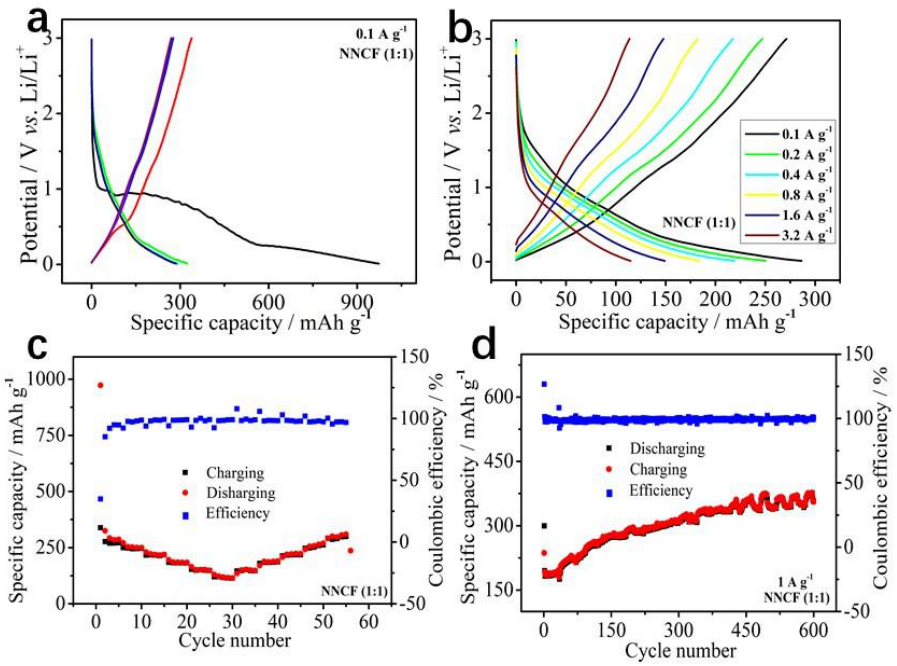

Figure S7. Performance of NNCF (1:1) electrode: GCD curves for the first five cycles at 0.1 A g^{-1} (a), GCD curves at 0.1-3.2 A g^{-1} (b), specific capacity and Coulombic efficiency at 0.1-3.2 A g^{-1} (c), and cycling behavior at 1 A g^{-1} (d).

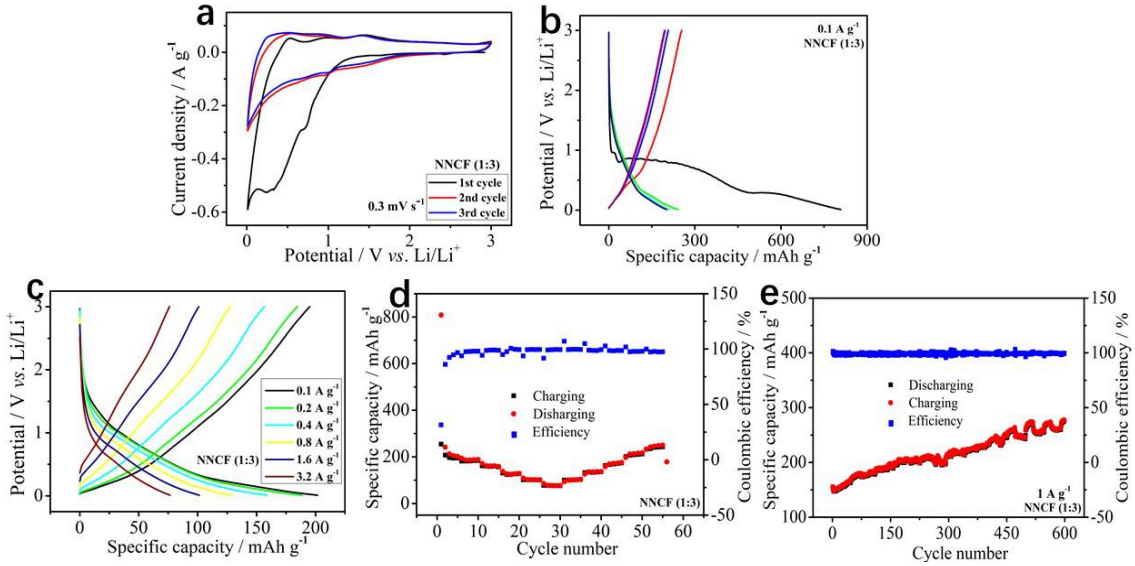

Figure S8. Performance of NNCF (3:1) electrode: CV plots for the first three cycles at 0.3 mV s^{-1} (a), GCD curves for the first five cycles at 0.1 A g^{-1} (b), GCD curves at 0.1-3.2 A g^{-1} (c), specific capacity and Coulombic efficiency at 0.1-3.2 A g^{-1} (d), and cycling behavior at1 A g^{-1} (e).

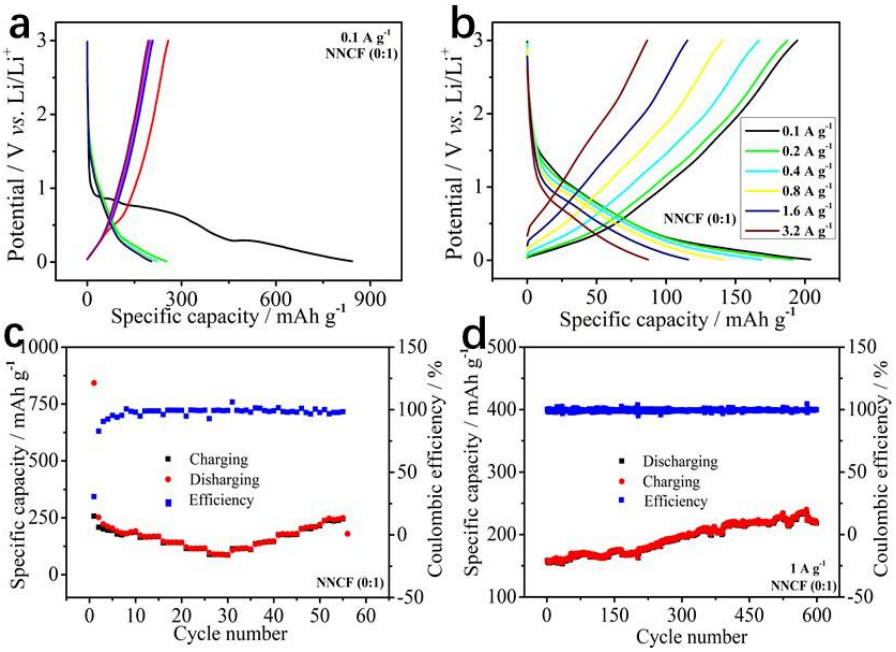

Figure S9. Performance of NNCF (0:1) electrode: GCD curves for the first five cycles at 0.1 A g^{-1} (a), GCD curves at 0.1-3.2 A g^{-1} (b), specific capacity and Coulombic efficiency at 0.1-3.2 A g^{-1} (c), and cycling behavior at 1 A g^{-1} (d).

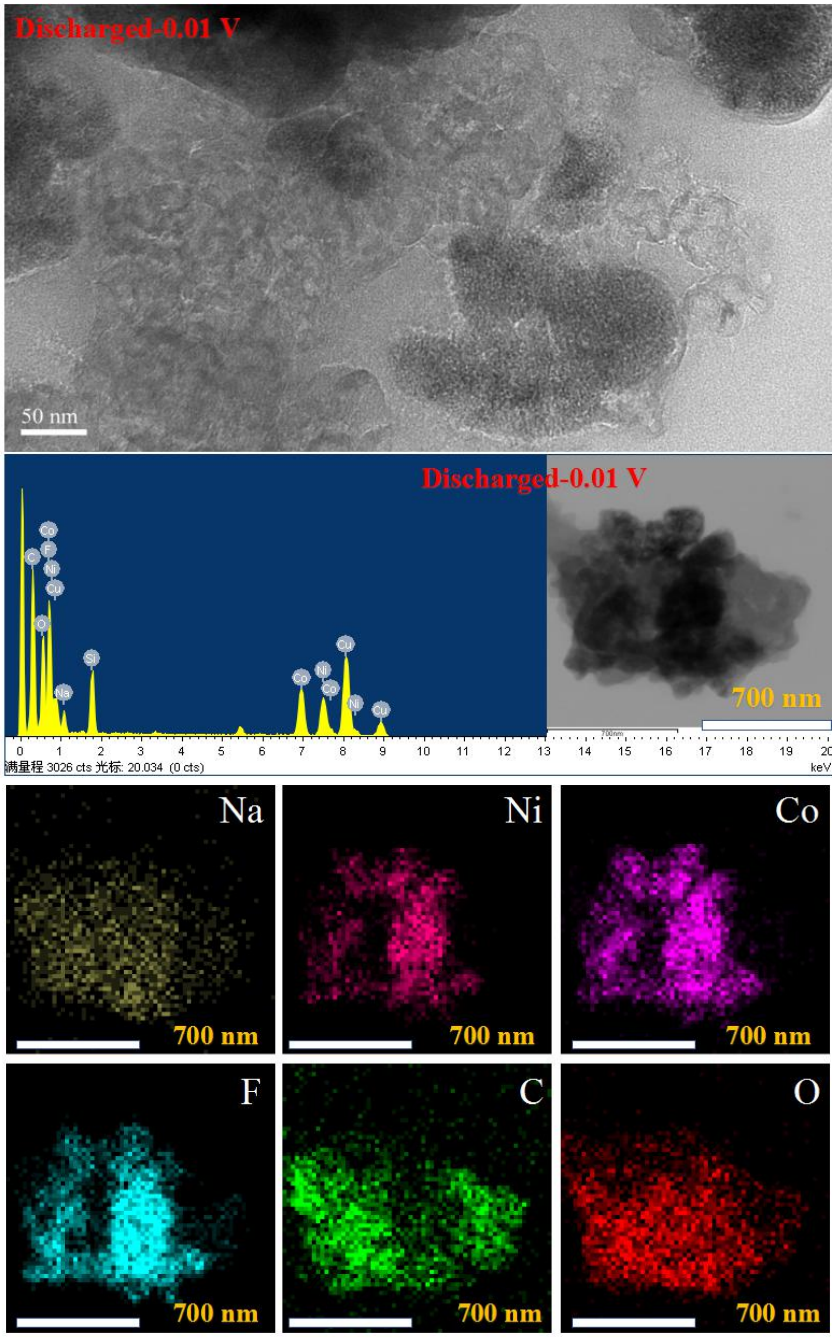

Figure S10. TEM images, EDS and mapping images of the NNCF (1:1) electrode in discharged-0.01 V state.

When fully discharged to 0.01 V, the NNCF (1:1) electrode undergone the dominant conversion reaction, and thus the amphorous Ni, Co, LiF, NaF phases and SEI films were formed. The ultrafine particle size of above-indicated amphorous phases can be detected by TEM images. The EDS patterns indicate the presence of Na, Ni, Co, F, C and O elements for the electrode in fully discharged state, and mapping images show the basically uniform distribution of these elements.

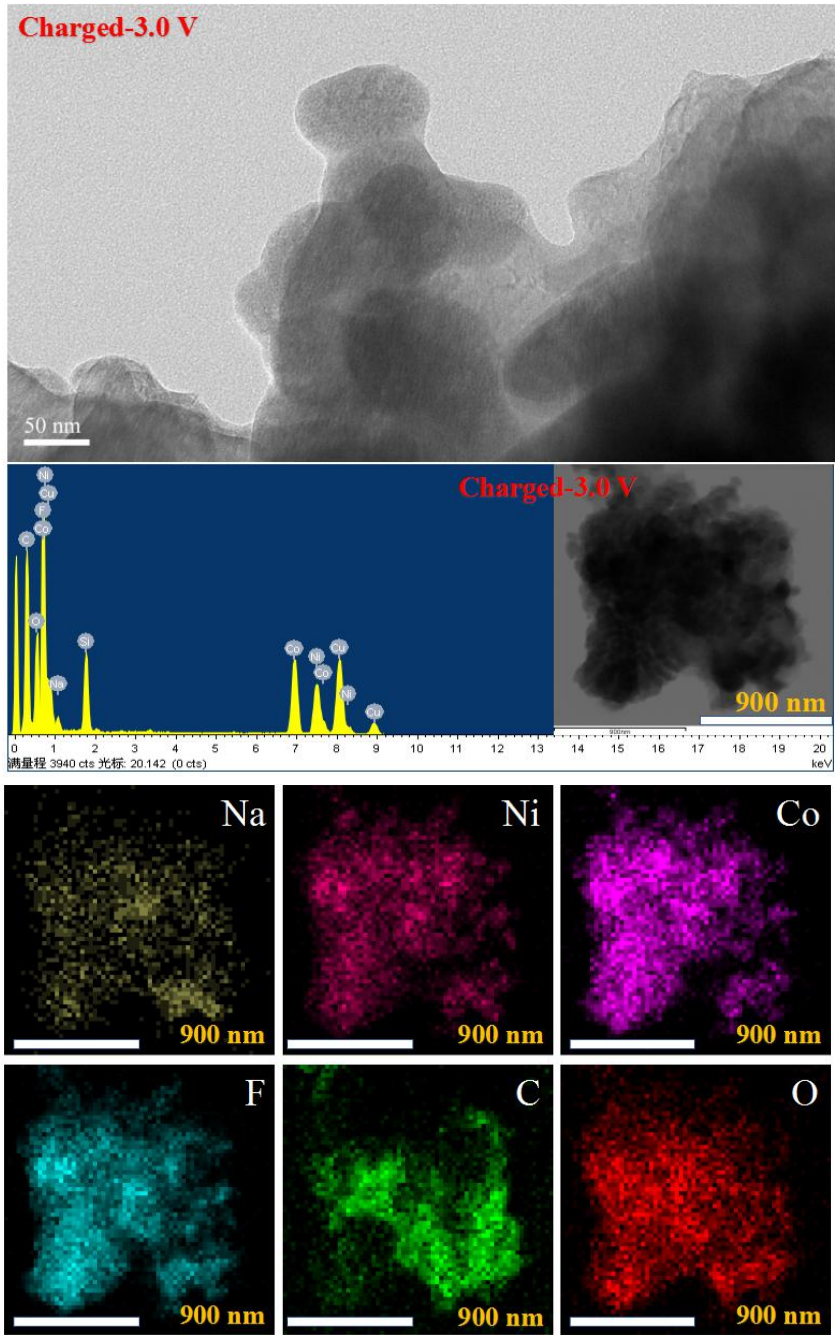

Figure S11. TEM images, EDS and mapping images of the NNCF (1:1) electrode in charged-3 V state.

When fully charged to 3.0 V, there are newly formed amphorous CoF_2, NiF_2 and incomplete reactants (Ni, Co, LiF, NaF) on the surface of the electrode. TEM images show the ultrafine particle size of the certain phases. The mapping images indicate a basically uniform distribution of Na, Ni, Co, F, C and O elements for the eletrode in charged-3 V state, and the elements of the fully charged state can be also detected by the EDS patterns.

a

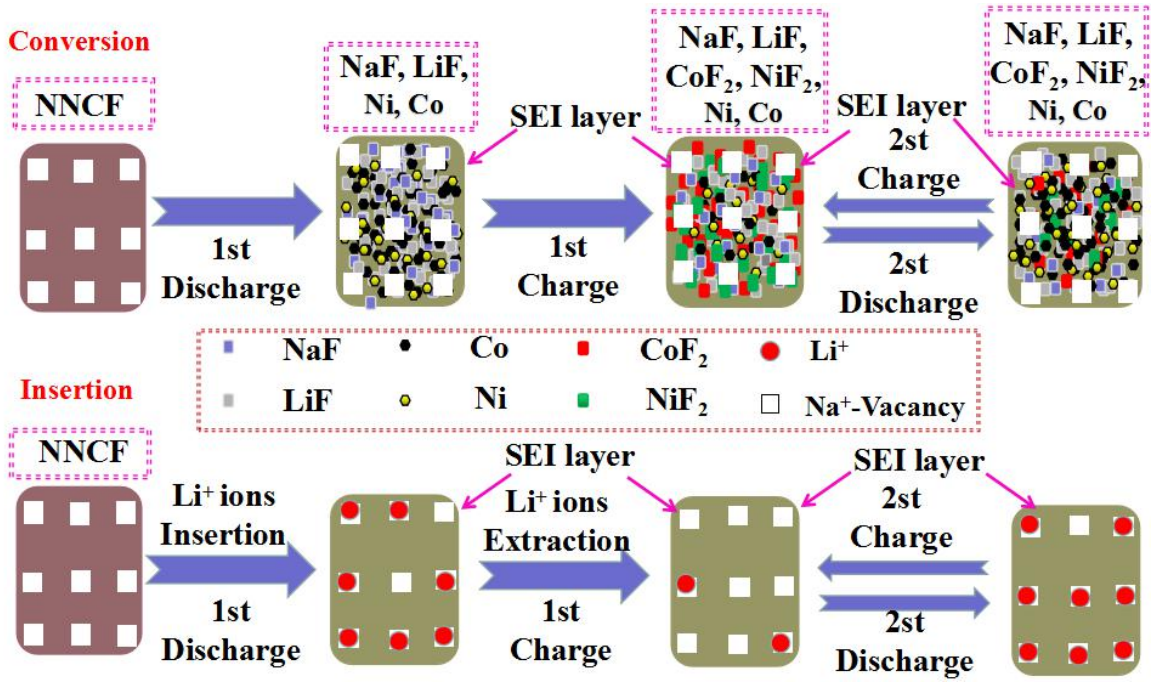

b

Phases	PDF Card	Crystal system	Space group	Cell (a x b x c) / Å^3
Ni	45-1027	Hexagonal	P63/mmc	2.651 X 2.651 X 4.343
Co	05-0727	Hexagonal	P63/mmc	2.503 X 2.503 X 4.061
NiF_2	24-0792	Tetragonal	P42/mnm	4.651 X 4.651 X 3.084
CoF_2	38-0883	Cubic	Pa3	4.958 X 4.958 X 4.958
LiF	45-1460	Cubic	Fm-3m	4.027 X 4.027 X 4.027
NaF	89-2956	Cubic	Fm-3m	4.634 X 4.634 X 4.634

Figure S12. Schematics of reaction mechanisms for NNCF (1:1) electrode during the discharging/charging processes under the first two cycles (a); Crystalline information of Ni, Co, NiF_2, CoF_2, NaF and LiF phases for the NNCF (1:1) electrode in charged-3 V and discharged-0.01 V states (b).

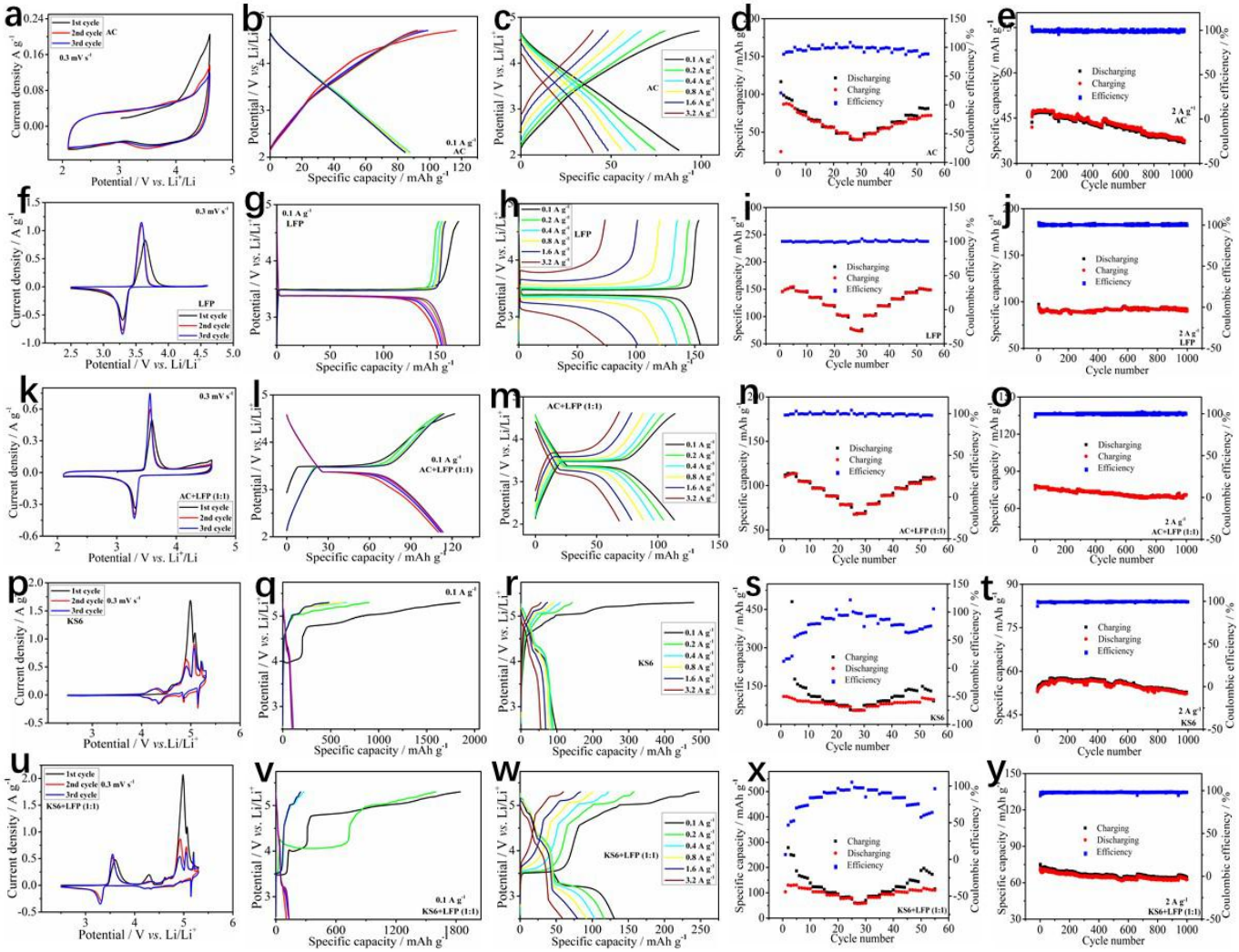

Figure S13. CV plots for the first three cycles at 0.3 mV s^{-1}, GCD curves for the first five cycles at 0.1 A g^{-1}, GCD curves at 0.1-3.2 A g^{-1}, specific capacity and Coulombic efficiency at 0.1-3.2 A g^{-1} and cycling behavior at 2 A g^{-1} of five types of positive electrodes: AC (a-e), LFP (f-j), AC+LFP (k-o), KS6 (p-t) and KS6+LFP (u-y).

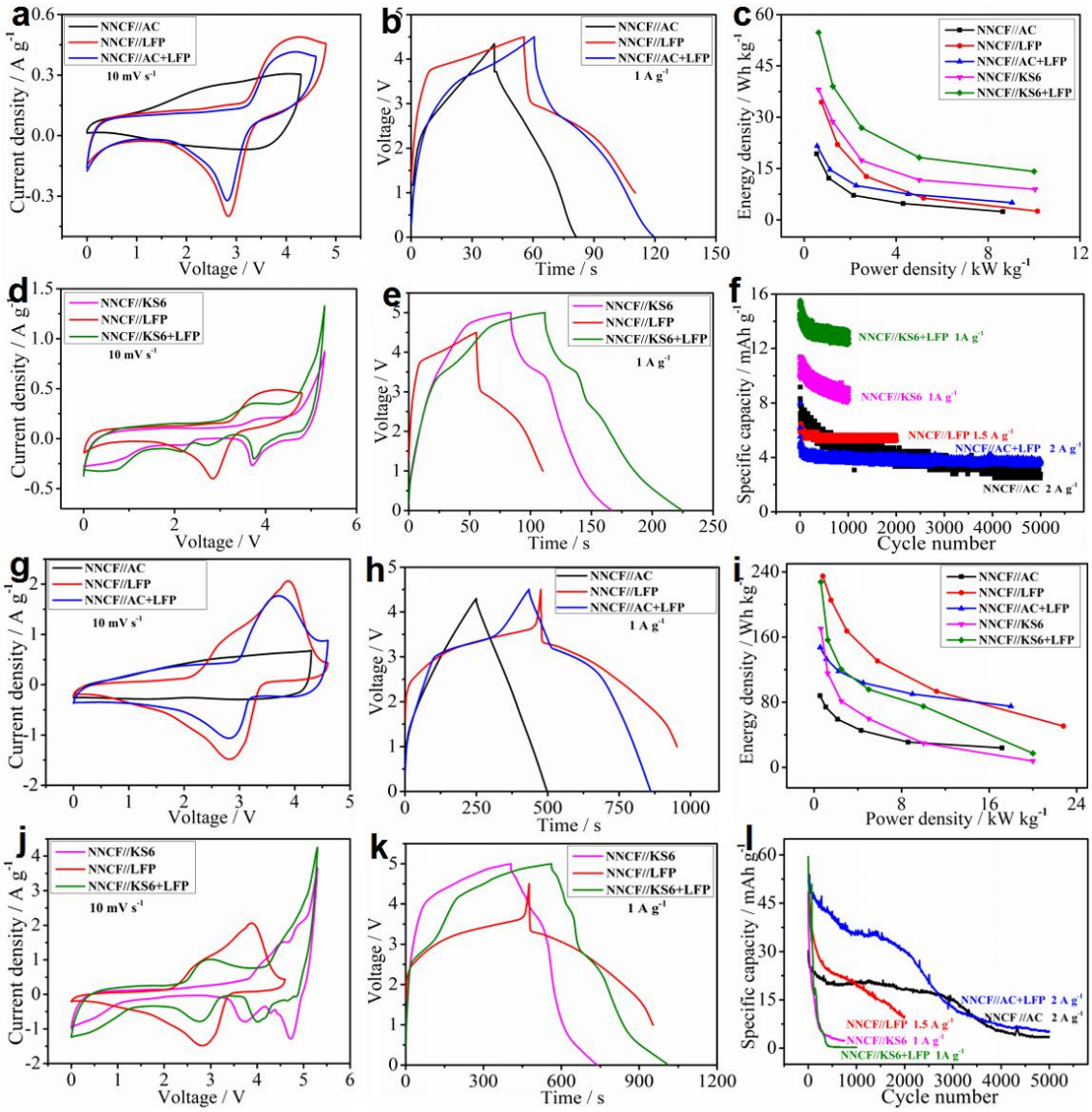

Figure S14. Performance of LICs (NNCF//AC, NNCF//AC+LFP), Li-DIBs (NNCF//KS6, NNCF//KS6+LFP) and LIB (NNCF//LFP) under low (-20 ℃) (a-f) and high (40 ℃) (g-l) temperatures: CV plots at 10 mV s^{-1} (a, d, g, j), GCD curves at 1 A g^{-1} (b, e, h, k), Ragone plots (c, i) and cycling behavior (f, l).

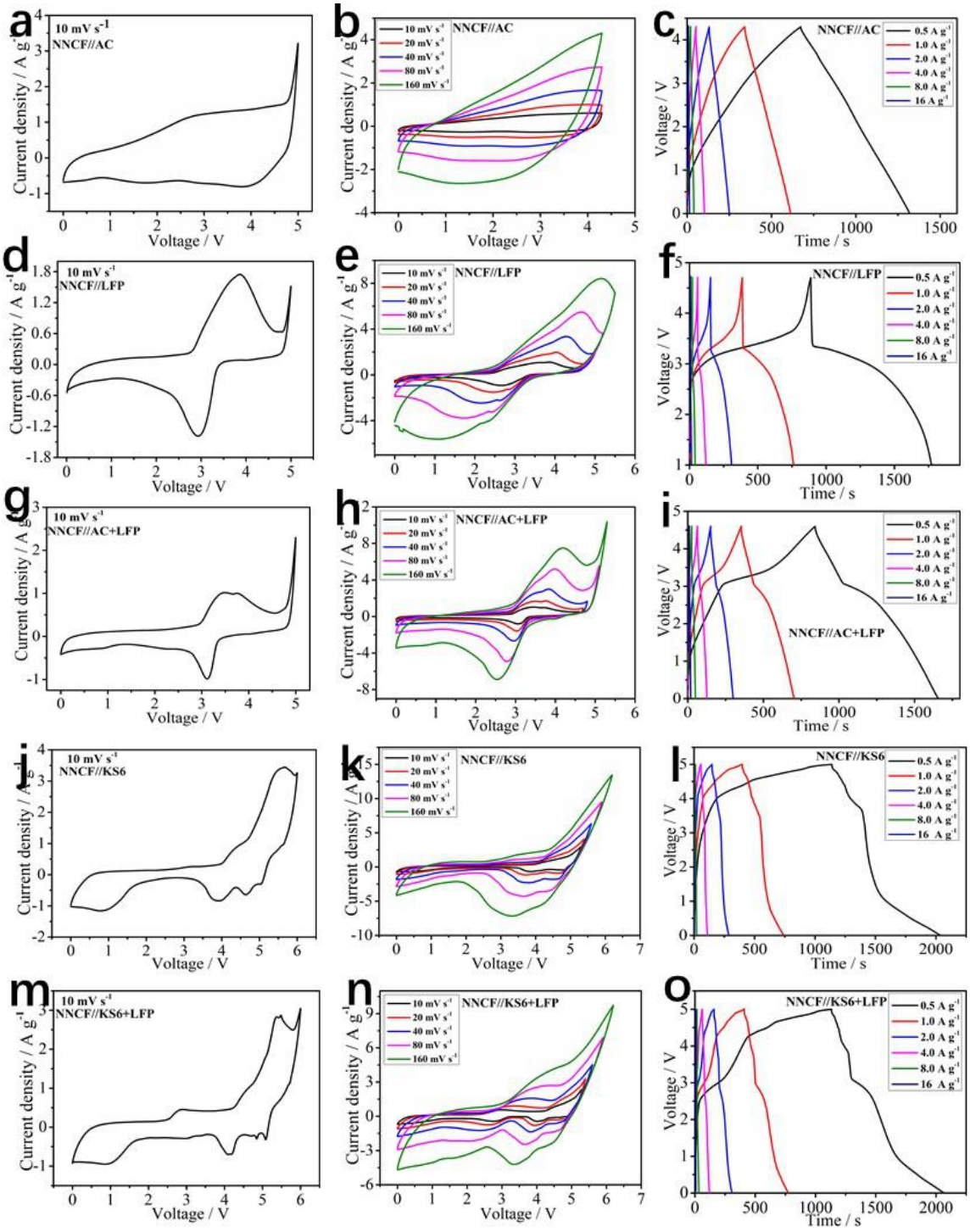

Figure S15. CV window at 10 mV s^{-1}, CV plots at 10-160 mV s^{-1} and GCD curves at 0.5-16 A g^{-1} under room temperature (25 °C) of LICs, Li-DIBs and LIBs in this work: NNCF//AC (a-c), NNCF//LFP (d-f), NNCF//AC+LFP (g-i), NNCF//KS6 (j-l) and NNCF//KS6+LFP (m-o).

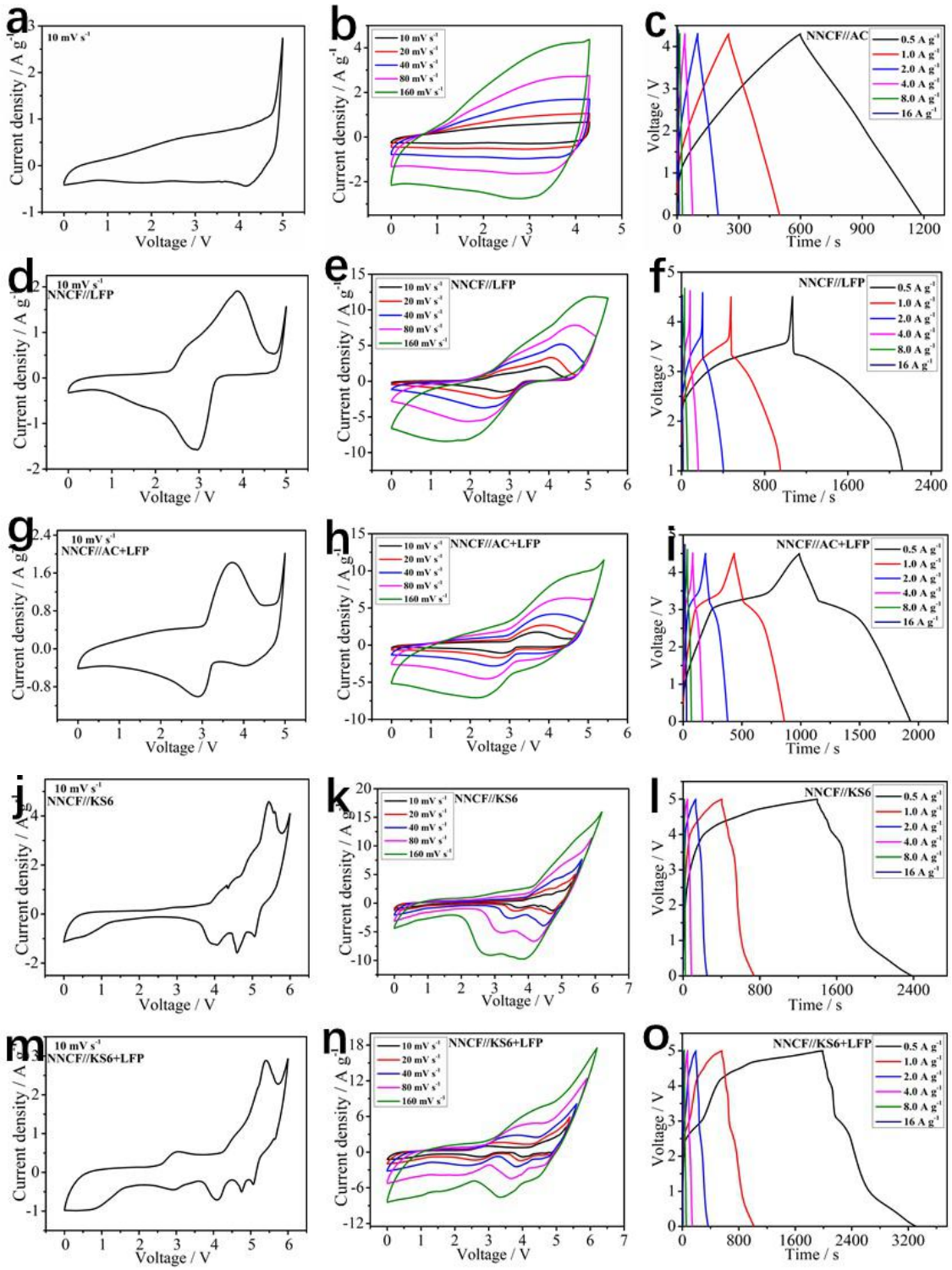

Figure S16. CV window at 10 mV s^{-1}, CV plots at 10-160 mV s^{-1} and GCD curves at 0.5-16 A g^{-1} under high temperature (40 ^{o}C) of LICs, Li-DIBs and LIBs in this work: NNCF//AC (a-c), NNCF//LFP (d-f), NNCF//AC+LFP (g-i), NNCF//KS6 (j-l) and NNCF//KS6+LFP (m-o).

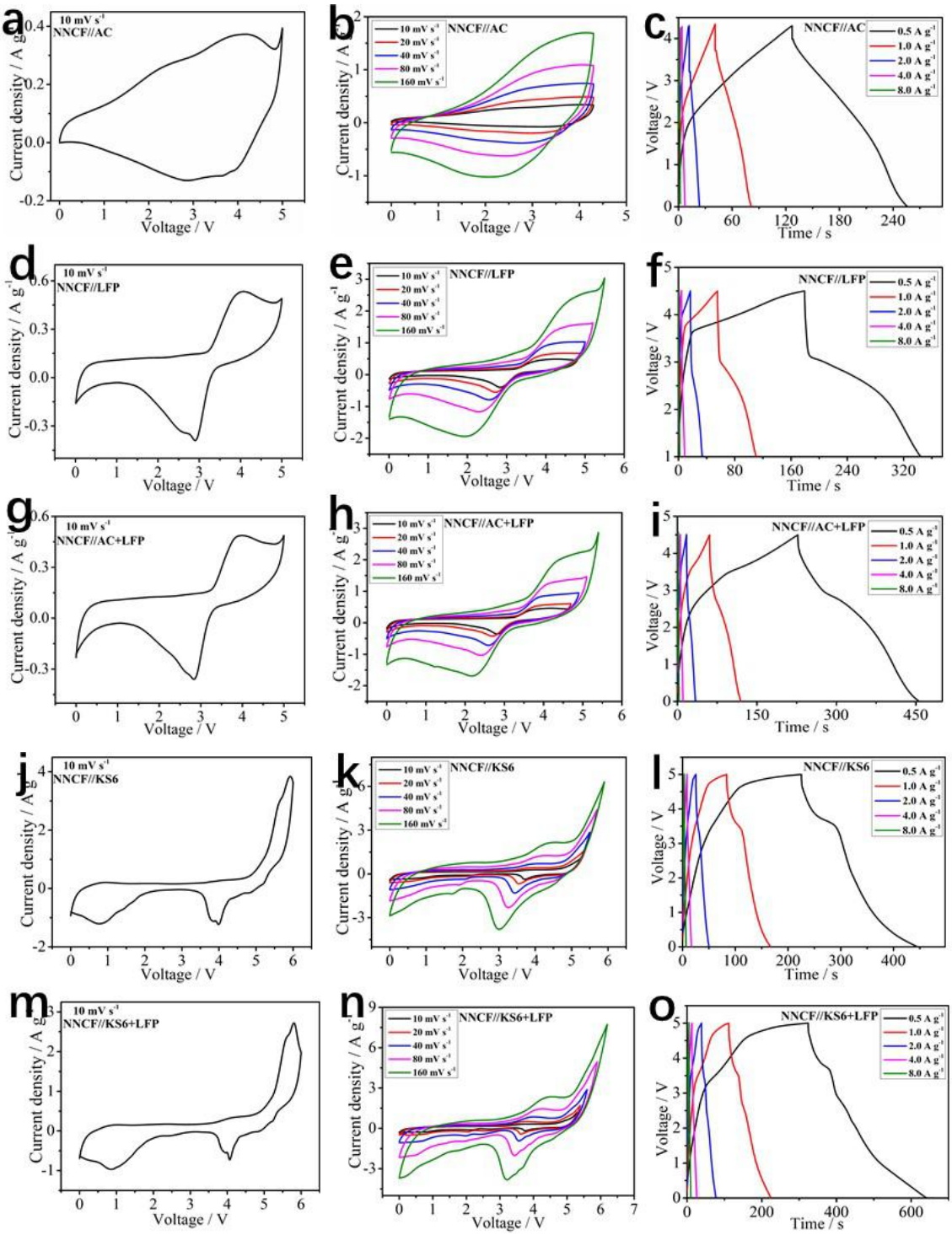

Figure S17. CV window at 10 mV s^{-1}, CV plots at 10-160 mV s^{-1} and GCD curves at 0.5-16 A g^{-1} under low temperature (-20 ^{o}C) of LICs, Li-DIBs and LIBs in this work: NNCF//AC (a-c), NNCF//LFP (d-f), NNCF//AC+LFP (g-i), NNCF//KS6 (j-l) and NNCF//KS6+LFP (m-o).

Table S1. Chemicals, agents and materials used in the study.

Chemials, Agents and Materials	Type	Company	Characteristics
$NiCl_2$•$6H_2O$	AR	SinoPharm	purity≥98.0%
$CoCl_2$•$6H_2O$	AR	SinoPharm	purity≥99.0%
NaF	AR	SinoPharm	purity≥98.0%
PVP-K30	GR	SinoPharm	purity≥99.8%
EG	AR	SinoPharm	purity≥99.0%
$LiFePO_4$	LFP-NCO	Aleees	D50: 4 ± 2 μm; Tab: 1 ± 0.2 g cm^{-3}; SSA:13 ± 2 m^2 g^{-1}
AC	YEC 8b	FuZhou YiHuan	D50: ~10 μm; Density: 0.4 g cm^{-3}; SSA:2000~2500 m^2 g^{-1}
Graphite	KS6	TiMCAL	D90: 5.8-7.1 μm; Interlayer distance: 0.3354-0.3360 nm; SSA: 20 m^2 g^{-1}; Density-Scott: 0.07 g cm^{-3};
AB	Battery grade		/
NMP	AR	Kermel	purity≥99.0%
PVDF	Battery grade		/
Electrolytes	LBC-305-01	CAPCHEM	1 M $LiPF_6$/EC:EMC:DMC (1:1:1) /1% VC
Li plate	15.6*0.45 mm	China Energy	15.6*0.45 mm
Cu foil	200*0.015	GuangZhou JiaYuan	Total thickness: 15 μm; weight: 87 g m^{-2}
Carbon coated-Al foil	222*0.015	GuagZhou NaNuo	Total thickness: 17 μm; Strength: 192 Mpa
Glass microfiber filters	GF/D 2.7 μm; 1823-025	Whatman	Diameter: 25 mm; Thickness: 675 μm; weight: 121 g m^{-2}
Cell components	CR-2032	ShenZhen TianChenHe	/

Table S2. Specific capacity and cycling retention of the NNCF (Ni:Co=1:0~0:1) electrodes.

	Specific capacity of NNCF electrodes (Ni/Co=1:0~0:1) / (mAh g^{-1})				
Current density / (A g^{-1})	**1:0**	**3:1**	**1:1**	**1:3**	**0:1**
0.1	255.4	267.5	286.3	200.8	203.9
0.2	203.3	242.3	250.2	188.7	191.3
0.4	171.4	212.2	219.1	161.2	168.6
0.8	137.5	174.8	183.7	127.0	141.7
1.6	108.4	136.5	149.0	105.2	115.9
3.2	78.3	102.6	114.8	78.9	87.0
Cycling behavior Retention% / 1 A g^{-1} / 600 cycles	220%	170%	187%	182%	140%

Table S3. Specific capacity cycling retention of AC, LFP, AC+LFP (1:1), KS6 and KS6+LFP (1:1) electrodes.

	Specific capacity of Positive electrodes / (mAh g^{-1})				
Current density / (A g^{-1})	**AC**	**LFP**	**AC+LFP**	**KS6**	**KS6+LFP**
0.1	84.8	154.6	113.4	98.2	130.5
0.2	72.1	146.1	104.6	90.3	116.4
0.4	63.8	135.0	96.6	85.8	103.4
0.8	56.2	120.2	88.0	80.0	91.9
1.6	48.5	101.3	78.6	69.0	79.6
3.2	40	73.2	68.4	54.9	59.3
Cycling behavior Retention% / 2 A g^{-1} / 1000 cycles	82%	98%	92%	98%	89%

Table S4. Performance summary of the LICs, Li-DIBs and LIBs in the study under room temperature (25 °C).

Type	Capacitor or Cell system	Working voltage / V	Energy density / Wh kg^{-1}	Power density / kW kg^{-1}	Cycling behavior / retention%, repeated cycles, current density
LICs	NNCF//AC	0.01-4.3	96.1-81.0 70.8-59.8 47.1-33.4	0.5-1.1 2.2-4.3 8.6-17.2	68%/1000/5 A g^{-1} 66%/2000/5 A g^{-1} 63%/3000/5 A g^{-1} 52%/5000/5 A g^{-1}
	NNCF//AC+LFP	0.01-4.6	132.3-113.4 97.4-81.3 67.9-53.1	0.6-1.1 2.3-4.6 9.2-18.4	82%/1000/5 A g^{-1} 79%/2000/5 A g^{-1} 74%/3000/5 A g^{-1} 66%/5000/5 A g^{-1}
LIBs	NNCF//LFP	1-4.7	196.2-161.6 128.3-95.1 63.5-35.2	0.8-1.6 3.1-5.8 11.2-19.2	74%/1000/3 A g^{-1} 63%/2000/3 A g^{-1} 56%/3000/3 A g^{-1}
Li-DIBs	NNCF//KS6	0.01-5.0	155.1-118.8 95.8-76.4 25.3-7.9	0.6-1.3 2.5-5.0 10-20.4	94%/100/2 A g^{-1} 67%/200/2 A g^{-1} 53%/300/2 A g^{-1} 45%/400/2 A g^{-1} 40%/500/2 A g^{-1} 26%/1000/2 A g^{-1}
	NNCF//KS6+LFP	0.01-5.0	161.3-126.4 103.4-82.0 41.1-17.2	0.6-1.2 2.5-5.0 9.9-20.7	91%/100/2 A g^{-1} 74%/200/2 A g^{-1} 63%/300/2 A g^{-1} 52%/400/2 A g^{-1} 44%/500/2 A g^{-1} 20%/1000/2 A g^{-1}

Table S5. Performance summary of the LICs, Li-DIBs and LIBs in the study under high (40 °C) and low (-20 °C) temperatures.

Type	Capacitor or Cell system	T / ℃	Working voltage / V	Energy density / Wh kg^{-1}	Power density / kW kg^{-1}	Cycling behavior / retention%, repeated cycles, current density
LICs	NNCF//AC	40	0.01-4.3	88.0-74.1 59.1-45.4 31.1-23.9	0.5-1.1 2.2-4.3 8.6-17.2	67%/1000/2 A g^{-1} 60%/2000/2 A g^{-1} 50%/3000/2 A g^{-1} 11%/5000/2 A g^{-1}
		-20	0.01-4.3	19.3-12.2 7.2-4.8-2.4	0.5-1.1 2.1-4.3-8.6	42%/500/2 A g^{-1} 42%/1000/2 A g^{-1} 37%/2000/2 A g^{-1}
	NNCF//AC+LFP	40	0.01-4.5	147.3-133.1 118.1-103.7 90.0-75.0	0.56-1.12 2.25-4.5 9.0-18.0	68%/1000/2 A g^{-1} 57%/2000/2 A g^{-1} 24%/3000/2 A g^{-1} 10%/5000/2 A g^{-1}
		-20	0.01-4.5	21.6-14.6 10.0-7.5-5.0	0.56-1.12 2.3-4.5-9.0	62%/500/2 A g^{-1} 47%/1000/2 A g^{-1} 45%/2000/2 A g^{-1}
LIBs	NNCF//LFP	40	1-4.5	234.8-205.3 167.5-130.6 93.3-50.7	0.8-1.5 3.0-5.8 11.2-22.8	63%/100/1.5 A g^{-1} 52%/200/1.5 A g^{-1} 41%/500/1.5 A g^{-1} 36%/1000/1.5A g^{-1} 17%/2000/1.5A g^{-1}
		-20	1-4.5	34.4-22.0 12.7-6.4-2.5	0.75-1.4 2.7-5.2-10.2	90%/1000/1.5A g^{-1} 89%/2000/1.5A g^{-1}
Li-DIBs	NNCF//KS6	40	0.01-5	170.1-115.3 81.2-59.7 29.6-7.8	0.6-1.25 2.5-5.0 10.0-20.0	78%/10/1 A g^{-1} 69%/20/1 A g^{-1} 50%/50/1 A g^{-1} 36%/100/1 A g^{-1} 16%/200/1 A g^{-1}
		-20	0.01-5	38.1-28.7 17.4-11.7-8.9	0.6-1.2 2.5-5.0-10.0	99%/500/1 A g^{-1} 91%/1000/1 A g^{-1}
	NNCF//KS6+LFP	40	0.01-5	227.6-156.4 120.1-95.8 75.0-17.2	0.6-1.25 2.5-5.0 10.0-20.0	87%/10/1 A g^{-1} 81%/20/1 A g^{-1} 64%/50/1 A g^{-1} 45%/100/1 A g^{-1} 16%/200/1 A g^{-1}
		-20	0.01-5	54.8-39.0 26.9-18.2-14.2	0.6-1.2 2.5-5.0-10.0	96%/500/1 A g^{-1} 90%/1000/1 A g^{-1}

Table S6. A comparison for the performance of the NNCF//AC and NNCF//AC+LFP LICs in the study with some reported LICs.

LICs	Working voltage / V	Energy density / Wh kg^{-1}	Power density / kW kg^{-1}	Cycling behavior / retention%, repeated cycles, current density	Refs.
Li_3VO_4/N-C//AC	1-4	136.4-24.4	0.53-11	87%/1500/2 A g^{-1}	1
$TiNb_2O_7$@C//CFs	0.8-3.2	110.4-20	0.1-5.46	77%/1500/0.2 A g^{-1}	2
MnO@C//PC	0.1-4	117.6-27.8	0.4-10.2	76%/5000/1 A g^{-1}	3
AC/TiO_2@PCNF-12	0-3	67.4-27.5	0.075-5	85%/10000/10 A g^{-1}	4
AC-HBP//LiC_6	2-3.9	100-20	0.3-2	70%/2000/0.5 A g^{-1}	5
TiO_2/graphene//AC	1-3	42-8.9	0.8-8	100%/6500/4 A g^{-1}	6
SnO_2-C//C	0.5-4.0	110-45	0.19-2.96	80%/2000/1 A g^{-1}	7
TiO_2 belt//Graphene	0-3.8	82-21	0.57-19	73%/600/1 A g^{-1}	8
Graphene-VN//cabron nanorods	0-4	162-64	0.2-10	83%/1000/2 A g^{-1}	9
T-Nb_2O_5/Graphene paper//AC	0.5-3	47-15	0.39-18	93%/2000/0.25 A g^{-1}	10
Fe_3O_4/Graphene// Graphene	1-4	147-86	0.15-2.5	70%/1000/2 A g^{-1}	11
NNCF//AC	**0.01-4.3**	**96.1-81.0 70.8-59.8 47.1-33.4**	**0.5-1.1 2.2-4.3 8.6-17.2**	**68%/1000/5 A g^{-1} 66%/2000/5 A g^{-1} 63%/3000/5 A g^{-1}**	**This work**
NNCF//AC+LFP	**0.01-4.6**	**132.3-113.4 97.4-81.3 67.9-53.1**	**0.6-1.1 2.3-4.6 9.2-18.4**	**82%/1000/5 A g^{-1} 79%/2000/5 A g^{-1} 74%/3000/5 A g^{-1} 66%/5000/5 A g^{-1}**	

Table S7. A comparison for the performance of the NNCF//LFP LIB in the study with some reported LIBs.

LIBs	Working voltage / V	Energy density / Wh kg^{-1}	Power density / kW kg^{-1}	Cycling behavior / retention%, repeated cycles, current density	Refs.
SLA1025 graphite//LCO	2.5-4.2	136	1.15		12
Graphene/Si multilayer// $LiNi_{1/3}Mn_{1/3}Co_{1/3}O_2$	3-4.3	156	0.03	70.4%/15/0.0375 A g^{-1}	13
TiO_2 nanofiber//LMO	1.7-2.5	220	0.314	90%/700/0.3 A g^{-1}	14
TiO_2 hollow nanofiber//LFP	0.9-2.5	165	0.16	88%/300/0.1 A g^{-1}	15
LTO//$LiNi_xCo_yMn_{1-x-y}O_2$	1.5-2.7	90	2.2		16
FeSb-TiC//LNMO	2.0-5.0	260	0.127	68%/50/0.0365 A g^{-1}	17
$Li_4Ti_5O_{12}$-$Li_2Ti_3O_7$// LFP	1.9-2.5	75	0.048		18
TiO_2(B) nanowires//$LiNi_{0.5}Mn_{1.5}O_4$	2.0-3.5	150	0.132	89%/100/0.5 C	19
Ni_3N nanosheets//LNMO	2.5-3.9	120	3.39	99%/250/1.4 A g^{-1}	20
NNCF//LFP	**1-4.7**	**196.2-161.6 128.3-95.1 63.5-35.2**	**0.8-1.6 3.1-5.8 11.2-19.2**	**74%/1000/3 A g^{-1} 63%/2000/3 A g^{-1}**	**This work**

Table S8. A comparison for the performance of the NNCF//KS6 and NNCF//KS6+LFP Li-DIBs in the study with some reported Li-DIBs.

Li-DIBs	Working voltage / V	Energy density / Wh kg^{-1}	Power density / kW kg^{-1}	Cycling behavior / retention%, repeated cycles, current density	Refs.
Graphite//Graphite	0.01-5.2	108		67%/50/0.05 A g^{-1}	21
Si-compound//Graphite	0-3	54		53%/100/0.1 A g^{-1}	22
Nb_2O_5//Graphite	1.5-3.5	52		84%/100/0.1 A g^{-1}	23
RGO// Graphite	0-4	70	1.33	74%/50/1.33 A g^{-1}	24
TiO_2//Graphite	1.5-3.7	36		88%/50/0.1 A g^{-1}	25
MoO_3//Graphite	1.5-3.5	77		90%/200/0.081 A g^{-1}	26
AC// Graphite	0-3.5	150		98% /100 /1.86 mA cm^{-2}	27
Graphite//Graphite	3-5	170		94%/500/0.5 A g^{-1}	28
Al//Graphite	3.0-5.0	150	1.2	98%/600/0.2 A g^{-1}	29
MTI//KS6-DIB	3.0-5.1	125	0.4	90%/200/0.5 A g^{-1}	30
NNCF//KS6	**0.01-5.0**	**155.1-118.8 95.8-76.4 25.3-7.9**	**0.6-1.3 2.5-5.0 10-20.4**	**94%/100/2 A g^{-1} 67%/200/2 A g^{-1}**	**This work**
NNCF//KS6+LFP	**0.01-5.0**	**161.3-126.4 103.4-82.0 41.1-17.2**	**0.6-1.2 2.5-5.0 9.9-20.7**	**91%/100/2 A g^{-1} 74%/200/2 A g^{-1} 63%/300/2 A g^{-1}**	

References

In Table S6

(1) Shen, L. F.; Lv, H. F.; Chen, S. Q.; Kopold, P.; van Aken, P. A.; Wu, X. J.; Maier, J.; Yu, Y. *Adv. Mater.* **2017**, *29* (27), 1700142.

(2) Wang, X. F.; Shen, G. Z. *Nano Energy* **2015**, *15,* 104–115.

(3) Yan, D.; Li, S. H.; Guo, L. P.; Dong, X. L.; Chen, Z. Y.; Li, W. C. *ACS Appl. Mater. Interfaces* **2018**, *10* (50), 43946–43952.

(4) Yang, C.; Lan, J. L.; Liu, W. X.; Liu, Y.; Yu, Y. H.; Yang, X. P. *ACS Appl. Mater. Interfaces* **2017**, *9* (22), 18710–18719.

(5) Jain, A.; Jayaraman, S.; Ulaganathan, M.; Balasubramanian, R.; Aravindan, V.; Srinivasan, M. P.; Madhavi, S. *Electrochim. Acta* **2017**, *228,* 131–138.

(6) Kim, H.; Cho, M. Y.; Kim, M. H.; Park, K. Y.; Gwon, H.; Lee, Y.; Roh, K. C.; Kang, K. *Adv. Energy Mater.* **2013**, *3* (11), 1500–1506.

(7) Qu, W. H.; Han, F.; Lu, A. H.; Xing, C.; Qiao, M.; Li, W. C. *J. Mater. Chem. A* **2014**, *2* (18), 6549–6557.

(8) Wang, H. W.; Guan, C.; Wang, X. F.; Fan, H. J. *Small* **2015**, *11* (12), 1470–1477.

(9) Wang, R. T.; Lang, J. W.; Zhang, P.; Lin, Z. Y.; Yan, X. B. *Adv. Funct. Mater.* **2015**, *25* (15), 2270–2278.

(10) Kong, L. P.; Zhang, C. F.; Wang, J. T.; Qiao, W. M.; Ling, L. C.; Long, D. H. *ACS Nano* **2015**, *9* (11), 11200–11208.

(11) Zhang, F.; Zhang, T. F.; Yang, X.; Zhang, L.; Leng, K.; Huang, Y.; Chen, Y. S. *Energy Environ. Sci.* **2013**, *6* (6), 1623–1632.

In Table S7

(12) Khomenko, V. G.; Barsukov, V. Z.; Doninger, J. E.; Barsukov, I. V. *J. Power Sources* **2007**, *165* (2), 598–608.

(13) Ji, L. W.; Zheng, H. H.; Ismach, A.; Tan, Z. K.; Xun, S. D.; Lin, E.; Battaglia, V.; Srinivasan, V.; Zhang, Y. G. *Nano Energy* **2012**, *1* (1), 164–171.

(14) Aravindan, V.; Sundaramurthy, J.; Kumar, P. S.; Shubha, N.; Ling, W. C.; Ramakrishna, S.; Madhavi, S. *Nanoscale* **2013**, *5,* 10636–10645

(15) Zhang, X.; Aravindan, V.; Kumar, P. S.; Liu, H. H.; Jayaraman, S.; Ramakrishna, S.; Madhavi, S. *Nanoscale* **2013**, *5* (13) 5973-5980.

(16) Takami, N.; Inagaki, H.; Tatebayashi, Y.; Saruwatari, H.; Honda, K.; Egusa, S. *J. Power Sources* **2013**, *244,* 469–475.

(17) Moorhead-Rosenberg, Z.; Allcorn, E.; Manthiram, A. *Chem. Mater.* **2014**, *26,* 5905–5913.

(18) Zhu, G. N.; Chen, L.; Wang, Y. G.; Wang, C. X.; Che, R. C.; Xia, Y. Y. Binary $Li_4Ti_5O_{12}$-$Li_2Ti_3O_7$ Nanocomposite as an Anode Material for Li-Ion Batteries. *Adv. Funct. Mater.* **2013**, *23* (5), 640-647.

(19) Armstrong, G.; Armstrong, A. R.; Bruce, P. G.; Reale, P.; Scrosati, B. *Adv. Mater.* **2006**, *18* (19), 2597–2600.

(20) Balogun, M. S.; Zeng, Y.; Qiu, W.; Luo, Y.; Onasanya, A.; Olaniyi, T. K.; Tong, Y. *J. Mater. Chem. A* **2016**, *4* (25), 9844–9849.

In Table S8

(21) Read, J. A.; Cresce, A. V.; Ervin, M. H.; Xu, K. *Energy Environ. Sci.* **2014**, *7* (2), 617–620.

(22) Nakano, H.; Sugiyama, Y.; Morishita, T.; Spencer, M. J. S.; Snook, I. K.; Kumai, Y.; Okamoto, H. *J. Mater. Chem. A* **2014**, *2* (20), 7588–7592.

(23) Park, G.; Gunawardhana, N.; Lee, C.; Lee, S. M.; Lee, Y. S.; Yoshio, M. *J. Power Sources* **2013**, *236,* 145–150.

(24) Shi, X. Y.; Zhang, W.; Wang, J. F.; Zheng, W. T.; Huang, K. K.; Zhang, H. B.; Feng, S. H.; Chen, H. *Adv. Energy Mater.* **2016**, *6* (24), 1–5.

(25) Thapa, A. K.; Park, G.; Nakamura, H.; Ishihara, T.; Moriyama, N.; Kawamura, T.; Wang, H.; Yoshio, M. *Electrochim. Acta* **2010**, *55* (24), 7305–7309.

(26) Gunawardhana, N.; Park, G. J.; Dimov, N.; Thapa, A. K.; Nakamura, H.; Wang, H.; Ishihara, T.; Yoshio, M. *J. Power Sources* **2011**, *196* (18), 7886–7890.

(27) Ishihara, T.; Yokoyama, Y.; Kozono, F.; Hayashi, H. *J. Power Sources* **2011**, *196* (16), 6956–6959.

(28) Rothermel, S.; Meister, P.; Schmuelling, G.; Fromm, O.; Meyer, H. W.; Nowak, S.; Winter, M.; Placke, T. *Energy Environ. Sci.* **2014**, *7* (10), 3412–3423.

(29) Zhang, X. L.; Tang, Y. B.; Zhang, F.; Lee, C. S. *Adv. Energy Mater.* **2016**, *6* (11), 1502588.

(30) Chan, C. Y.; Lee, P. K.; Xu, Z. H.; Yu, D. Y. W. *Electrochim. Acta* **2018**, *263,* 34–39.